Supporting Information for

Metabolism, survival, and gene expression of *Pseudomonas putida* to hematite nanoparticles mediated by surface-bound humic acid

Kai Ouyang[a], Sharon L. Walker[b], Xiao-Ying Yu[c], Chun-Hui Gao[a], Qiaoyun Huang[a], Peng Cai[a,*]

[a]State Key Laboratory of Agricultural Microbiology, College of Resources and Environment, Huazhong Agricultural University, Wuhan 430070, China

[b]Department of Chemical and Environmental Engineering, University of California, Riverside, California 92521, USA

[c]Earth & Biological Sciences Directorate, Pacific Northwest National Laboratory, Richland, WA 99354 USA

*Corresponding author: Peng Cai

State Key Laboratory of Agricultural Microbiology

Huazhong Agricultural University, Wuhan, China

Phone: +86 27 87671033; Fax: +86 27 87280670

E-mail address: cp@mail.hzau.edu.cn

Additional Materials and Methods

Hematite Synthesis. The hematite nanoparticles were synthesized by slowly dripping 80 mL of 1 M ferric nitrate solution at the speed of 0.5 mL min^{-1} into 1 L of boiling distilled Milli-Q water while stirring vigorously. After the dripping was finished, the resulting suspension was removed from the heat and cooled overnight. The suspension was then dialyzed in standard grade Cellulose dialysis membranes (1000 MWCO, Spectra Por) against MilliQ water until the conductivity remained constant. The suspension was centrifuged (Eppendorf centrifuge 5430R, Germany) at 5000 g for 30 min, and the supernatant was discarded. Finally, the concentrated NPs were vacuum freeze-dried and ground to uniformity, and then stored in suspensions at 4 ◦C in dark.

Method for Humic acid (HA) Purification[1]. HA of 100 g was dissolved into 1 L of 0.1 M NaOH after mixing (180 rpm) for 12 h at room temperature (adjusting the solution to pH 10 before stirring). $Na_2SO_4 \cdot 10H_2O$ was added into the resultant solution to remove the possible inorganic colloids overnight. The solution was then centrifuged at 6000 g for 15 min and the supernatant was collected for acidification (pH 1-1.5 with 3 M HCl) to obtain the HA fraction. The acidified solution was centrifuged at 6000 g for 15 min and the precipitate was collected and mixed with 100 mL of mixed acid (0.5 mL concentrated HCl + 0.5 mL 48% HF + 99 mL H_2O). The mixed suspension was shaken for 5 h and followed by centrifugation at 6000 g for 15 min. The precipitate obtained was rinsed twice with ultrapure water from a Milli-Q system, centrifuged, vacuum-dried at 40 °C, gently ground to pass through a 100-mesh sieve, and stored for subsequent use.

The Composition of Modified Minimal Davis (MMD) Media. Basic

characterization and all toxicological assays of NPs were conducted on cultures grown in an environmentally-relevant media, Modified Minimal Davis (MMD) media [1 L of H_2O containing 0.7 g of K_2HPO_4, 0.2 g of KH_2PO_4, 0.66 g of $(NH4)_2SO_4$, 0.5 g of sodium citrate, 0.1 g of $MgSO_4 \cdot 7H_2O$, and 3.31 g of D-glucose at pH 6.9].[2] The MMD media was prepared and autoclaved. The D-glucose solution was autoclaved separately.

ROS Measurement. The generation of intracellular ROS was determined using the fluorescence probe 2',7'-dichlorodihydrofluorescein diacetate (DCFH-DA, Sigma-Aldrich, USA) and followed the procedure described by Saison et al.[3] Briefly, 1.5 mL of the treated (expose to NPs) or untreated (control, without NPs) cell suspensions were collected after centrifugation (5000g, 10 min), washed twice with PBS buffer solution, incubated with 10 mM DCFH-DA for 30 min in the dark, and washed with PBS again. Since DCFH-DA could be transformed into 2',7'-dichlorodihydrofluorescein (H2DCF) by intracellular esterase if they enter cells. When intracellular ROS generated, 2',7'-dichlorofluorescein (DCF) would be converted from H2DCF. Thus the fluorescence intensity (FI) of DCF was measured with a fluorescence pate reader using an excitation of 480 nm and an emission of 520 nm, which indicated the extent of ROS generation. The formula to evaluate ROS levels followed the method proposed by Hong et al.[4] Changes in ROS levels as compared to the control were evaluated using eq 1.

$$\text{Relative ROS level (\%)} = (FI_{NP} / FI_{Control}) \times 100 \quad (1)$$

where FI_{NP} and $FI_{Control}$ represent the mean fluorescence intensity of DCF from the cell suspensions system treated with NPs and untreated system, respectively.

MDA Measurement. Malondialdehyde (MDA), a major end-product and an index of lipid peroxidation, was measured using the thiobarbituric acid method.[5,6] The treated *P. putida* cells were collected and incubated with 2 ml of 10% (w/v) trichloroacetic acid for 1 h at 25 °C, and then 1 ml of 0.6% (w/v) 2-thiobarbituric acid (in 10% trichloroacetic acid) was added. The mixture was heated for 15 min at 100 °C in a water bath and cooled quickly to stop the reaction. The mixture was centrifuged at 5000 rpm for 15 min and the supernatant was collected. The absorbance was read at 532, 600 and 450 nm. MDA level was calculated by $\{6.45\times(OD_{532}-OD_{600})-0.56\times OD_{450}\} \times 3$ (reaction volume)/total cell number (10^8 cells). The relative MDA rates were calculated by the relative MDA contents of the *P. putida* cells under the different treatments (expose to hematite or hematite-HA complexes) compared to the blank controls (without NP), respectively.

Quantitative real-time PCR analyses. The quantitative polymerase chain reaction (qPCR) primers were designed by using online software tools Primer 3 and Beacon Designer 7. The primer sequences with the product lengths are listed in Table S1. The qPCR was performed in a real-time PCR system (ABI ViiA™ 7). The reaction mix was prepared with 5 μL iTaq™ Universal SYBR green supermix (BIO-RAD), 2μL each of forward and reverse primers, 1μL cDNA, and 2μL of nuclease-free water. The qPCR program for the reaction was 95 °C for 30 s, 40 cycles of 95 °C for 10 s, and 55 °C for 20 s, with a final temperature of 60 °C for 35 s. To confirm specific

amplification of the PCR product, melting curve analysis was carried out for 40min. The experiment was carried out in 3 biological replicates, and each replicate was analyzed in duplicate. Constitutively expressed gapA genes were used as an internal control. A standard graph was plotted for each gene with gapA as the endogenous control. Fold change in gene expression was calculated with respect to control, and statistical significance was determined at $p<0.05$.

Additional Results and Discussion

Characterization of the Hematite Nanoparticles and Hematite Nanoparticles-HA Complexes. The powder X-ray diffraction (XRD) pattern of the synthetic nanoparticles (SI Figure SI-2) revealed that only hematite phase was present. As expected, the crystal structure of hematite was not changed after modification with HA. The average diameter of the individual uncoated hematite nanoparticles measured by TEM was 10±5 nm (SI Figure SI-1). In contrast to the clear surfaces and sharp edges of the uncoated hematite (SI Figure SI-1A), the edges of hematite-10%HA were less well defined likely due to the form of HA-coating. More generally, the NP-HA complex exhibited a greater degree of aggregation than the uncoated NPs (SI Figure SI-1B).

FTIR spectra of the hematite-HA complexes are shown in SI Figure SI-3. The absorption bands in the range 400-750 cm^{-1} represent Fe-O vibration mode of Fe_2O_3.[7,8] The vibrational bands at around 3420 cm^{-1} and 1620 cm^{-1} corresponds to the flexural vibration of hydroxyl groups. The strong peaks at 1384 cm^{-1} indicated rich hydroxyl groups on the surfaces of bare hematite, however, the peak significantly

decreased after HA-coating. And a new peak around 1390 cm^{-1} appeared and increased with the HA-coating, suggesting the formation of ferri-acetate complexation between -COOH of HA and Fe of hematite.

Table S1. Sequence of quantitative PCR primers.

Primer name	Sequence
ddcA forward	5’- TTGATGATGGCGTGGT
ddcA reverse	5’-ATTTCCGTGACCCACA
ppuI forward	5’-ATGCATAAACTTCGGGCA
ppuI reverse	5’-CATTTTCTCGACCCCCAC
qseB forward	5’-ACGTGATGATCCTCGACCTC
qseB reverse	5’-GGCTTGAGCAGGTAATCGTC
qseC forward	5’-GACAATCGGCGTATCCTGTT
qseC reverse	5’-ATCTGCACCTCCAACTCCAC
hfQ forward	5’-AAAGGGCATTCGCTACAAGA
hfQ reverse	5’-TGTAGACCATCTGGCTGACG
pp0806 forward	5’-GTCCCTTACCAGACCAACGA
pp0806 reverse	5’-TGGCACCAGTGTTATTTGGA
wbpL forward	5’-GCCATCGGTTTGCTGTATTT
wbpL reverse	5’-GCATGACCAGTGAGCCAGTA
wbpY forward	5’-AGTTCCATCCTCGGACTCCT
wbpY reverse	5’-AGCCATGATACCCACTGAGG
wbpZ forward	5’-CCGACATTGTGCACTACCAC
wbpZ reverse	5’-CAACGGCTGATACAGCTTGA
OmlA forward	5’-CACCAATCGTTGGGATTACC
OmlA reverse	5’-CAGACAGGCTGACCAGTTGA

fepA forward	5’-GTGAGTGCCGGGTACAAGTT
fepA reverse	5’-GATATTCAGCGCAGCAAACA
murF forward	5’-AATGTGCTGGGTGAACACAA
murF reverse	5’-CGCACATAGAGGTGGGATTT
oprD forward	5’-GCTGAAAGTGGGTGACCAGT
oprD reverse	5’-CAGTCAGGCTGGTGAAGTGA
fpr forward	5’-AAACCTACGAGCGCTTTGAA
fpr reverse	5’-GGTCACGGTCGGGTAGTAGA
soxR forward	5’-TGTCTGCGCTGCACTTCTAC
soxR reverse	5’-TAACGGCTGAAGGCTTGTTT
sodA forward	5’-CAGCCTGTTCTGGACTGTCA
soda reverse	5’-CTTTGGTGAAAGCCTCCTTG
sodB forward	5’-GACCCTGGAAGAGATCGTCA
sodB reverse	5’-CTTGTCGAAGGAACCGAAAG
ahpC forward	5’-AGGCCAGATCAAGATTGTCG
ahpC reverse	5’-CTTCGCCTTCTTTCCACTTG

Table S2. The 24 h LC_{50} of test NPs to *P. putida,* the magnitude of interaction energy barrier between hematite NPs and cell surface

Test substances	LC_{50} (mg L^{-1})	energy barrier (kT^{a})
hematite	23.58	6.93
hematite-0.2%HA	197.29	7.26
hematite-1%HA	724.83	7.38
hematite-2%HA	987.59	7.65
hematite-10%HA	4774.23	8.91

Table S3. The peak time (PT), peak height (PH), growth rate constant (*k*) and total heat output (Q) of *Pseudomonas putida* influenced by various nanoparticles

(The concentration of nanoparticles is 500 mg L^{-1}.)

	PT (h)	PH (μW)	Q (J)	*k* (min^{-1})	R^2
Control	9.8	372.2±1.7[a]	15.666±0.006[a]	0.452±0.005[a]	0.994
hematite-10%HA	10.4	361.4±0.8[b]	13.149±0.014[b]	0.437±0.001[b]	0.992
hematite-2%HA	11.3	357.8±0.7[c]	11.336±0.005[c]	0.440±0.006[a]	0.982
hematite-1%HA	11.8	355.2±0.2[d]	11.092±0.007[d]	0.387±0.005[c]	0.972
hematite-0.2%HA	12.9	348.7±0.5[e]	10.885±0.006[e]	0.376±0.006[d]	0.969
hematite	11.0	227.6±0.5[f]	10.438±0.006[f]	0.289±0.004[e]	0.941

Table S4. Statistical analysis of the relative ROS and MDA contents of the *P. putida* cells under the different treatments (P<0.05).

Test substances	Relative ROS rate (%)	Relative MDA rate (%)
hematite	7622.2±715.5^{b}	1122.9±10.3^{a}
hematite-0.2%HA	9151.2±538.9^{a}	953.5±15.9^{b}
hematite-1%HA	7261.4±420.1^{b}	905.8±28.5^{c}
hematite-2%HA	5580.8±360.1^{c}	706.8±4.1^{d}
hematite-10%HA	1838.6±106.7^{d}	488.7±9.3^{e}

Table S5. The exponential model-fitted parameters of the settling curves

Test substances	$OD_{plateau}$	OD_1	R_0 (min^{-1})	R^2
P. putida	0.872±0.000	0.120±0.000	0.034	0.949
hematite	0.234±0.003	0.688±0.007	0.175	0.943
hematite-0.2%HA	0.380±0.002	0.630±0.002	0.138	0.948
hematite-1%HA	0.423±0.000	0.576±0.006	0.094	0.981
hematite-2%HA	0.497±0.005	0.498±0.000	0.081	0.983
hematite-10%HA	0.427±0.004	0.596±0.001	0.046	0.945
hematite/*P. putida*	0.402±0.005	0.499±0.004	0.224	0.965
hematite-0.2%HA/*P. putida*	0.454±0.010	0.555±0.009	0.173	0.965
hematite-1%HA/*P. putida*	0.654±0.056	0.313±0.005	0.133	0.952
hematite-2%HA/*P. putida*	0.746±0.002	0.199±0.001	0.103	0.948
hematite-10%HA/*P. putida*	0.750±0.002	0.183±0.008	0.083	0.988

$OD_{plateau}$ represent the optical density (OD = Absorbance (t) / Absorbance (0)), t is the settling time (min).

OD_1 represent the reduced OD where the settling curve plateaus.

R_0 is the settling rate.

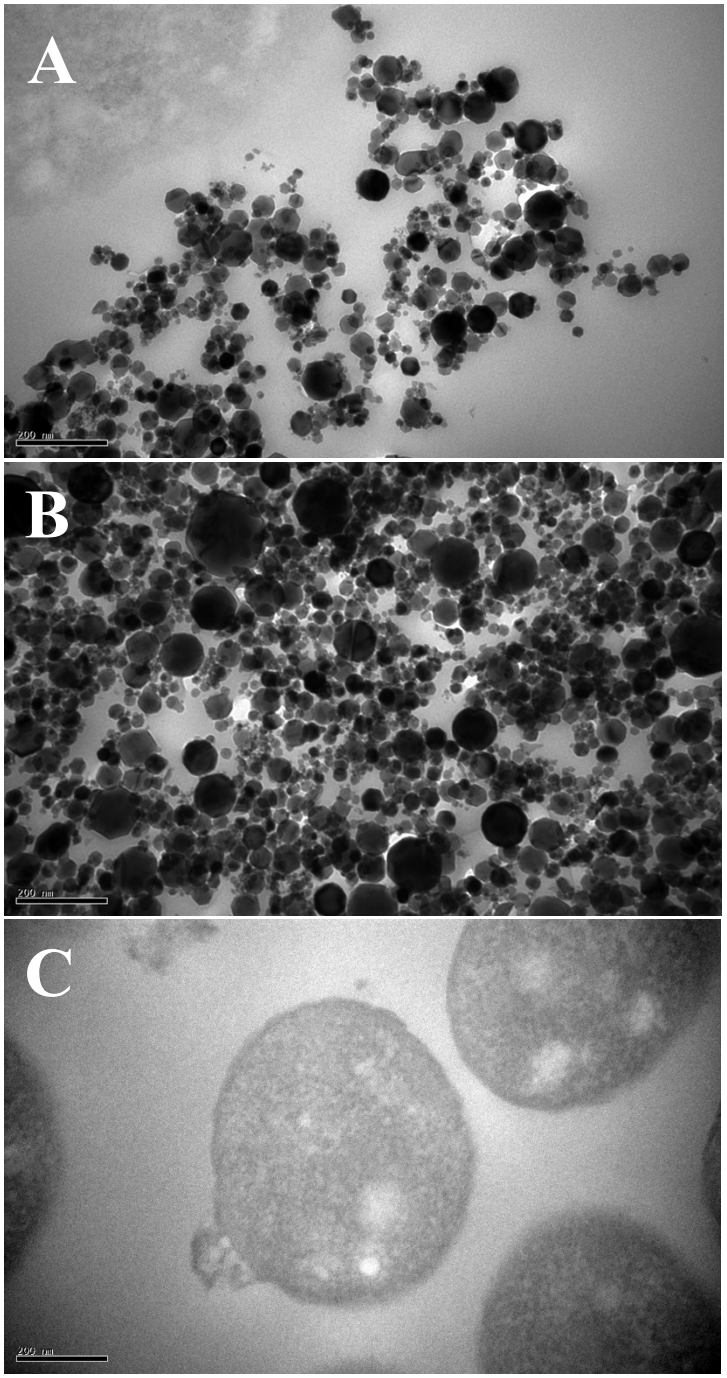

Figure S1 TEM images of (A) hematite, (B) hematite-HA complexes, and (C) *P. putida*.

(The scale bar for each image is 200 nm.)

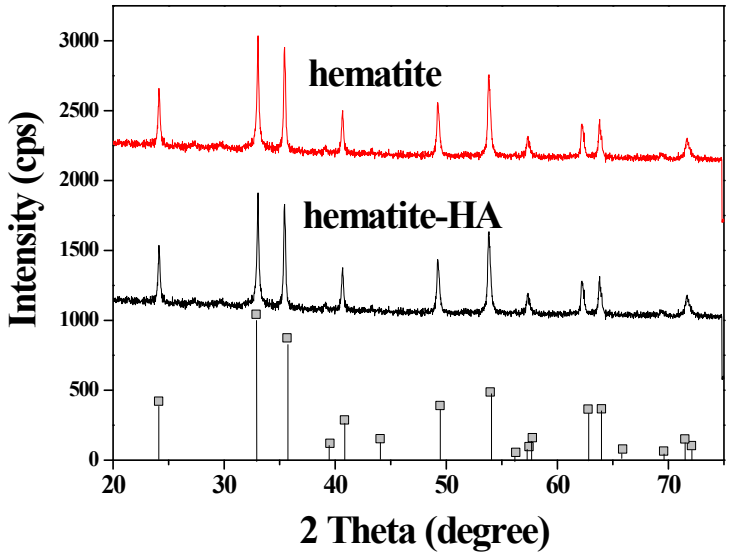

Figure S2 XRD patterns of the hematite and hematite-HA complexes.

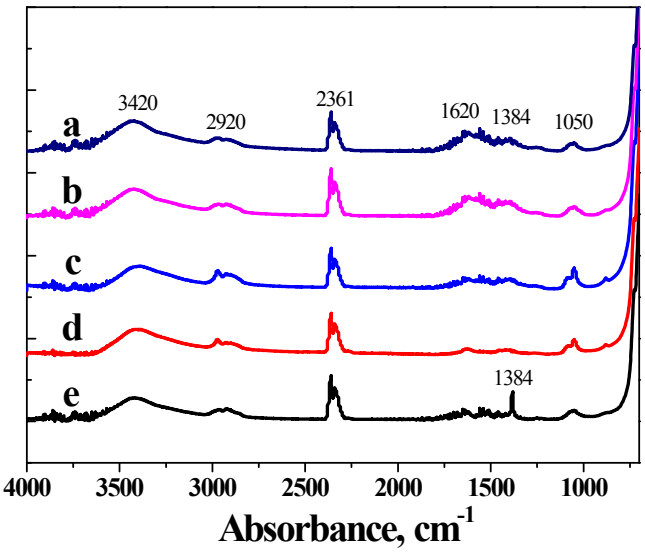

Figure S3 FTIR spectra of (a) hematite-10%HA, (b) hematite-2%HA, (c) hematite-1%HA, (d) hematite-0.2%HA, (e) hematite.

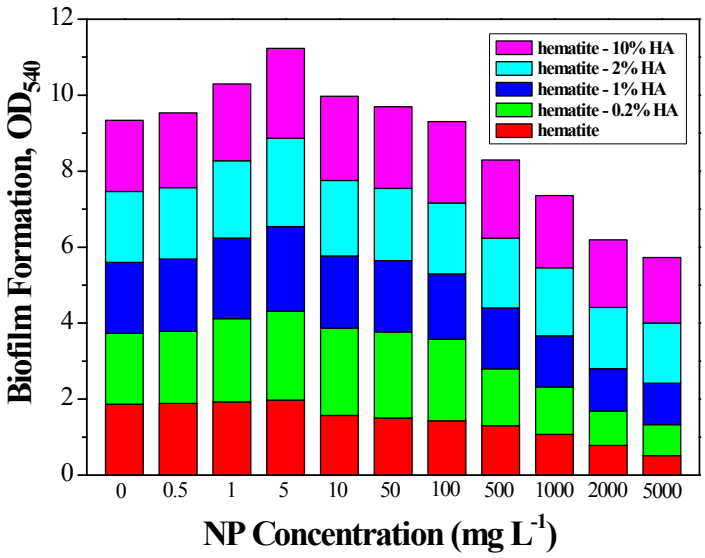

Figure S4 Effects of different hematite and the hematite-HA complexes concentrations on the biofilm development of *P. putida* (0, 0.5, 1, 5, 10, 50, 100 mg L^{-1}).

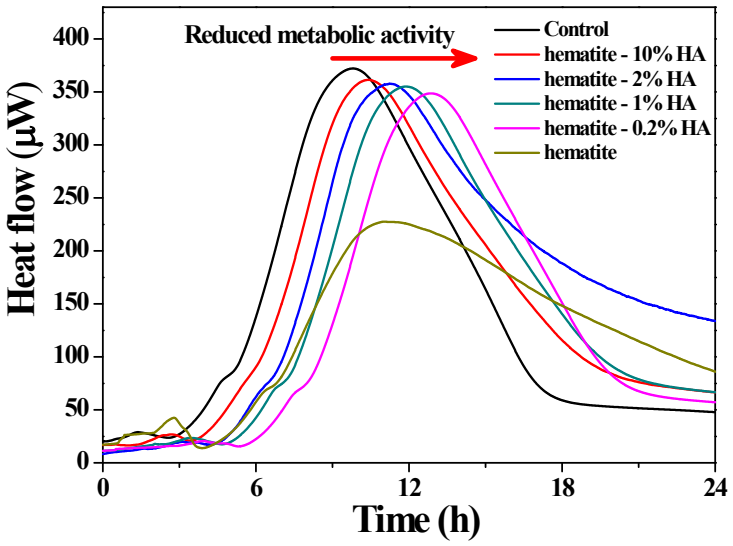

Figure S5 The power-time curves of *P. putida* in the presence of hematite and the hematite-HA complexes.

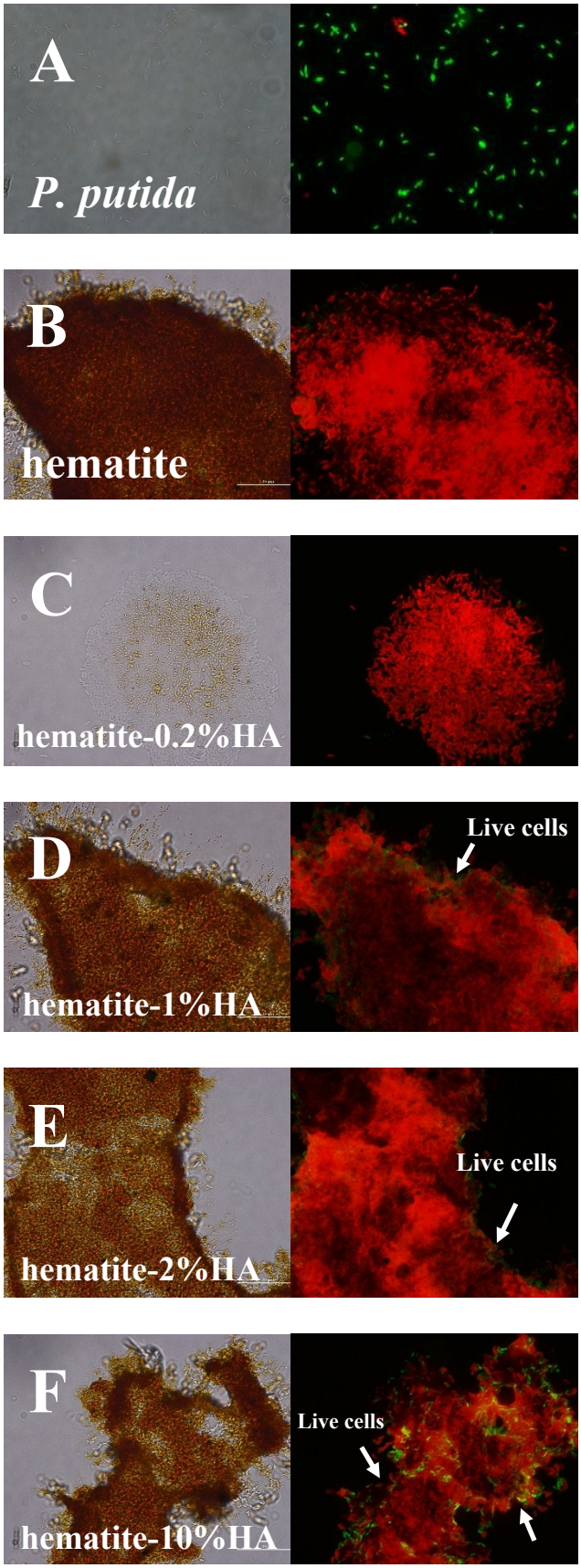

Figure S6 Fluorescent microscopy images of LIVE/DEAD stained *P. putida* grown for 24 h in the (A) absence of hematite, presence of (B) hematite, (C) hematite-0.2%HA complexes, (D)

hematite-1%HA complexes, (E) hematite-2%HA complexes, (F) hematite-10%HA. (The scale bar for each image is 20 μm; red-dead cells, green-live cells.)

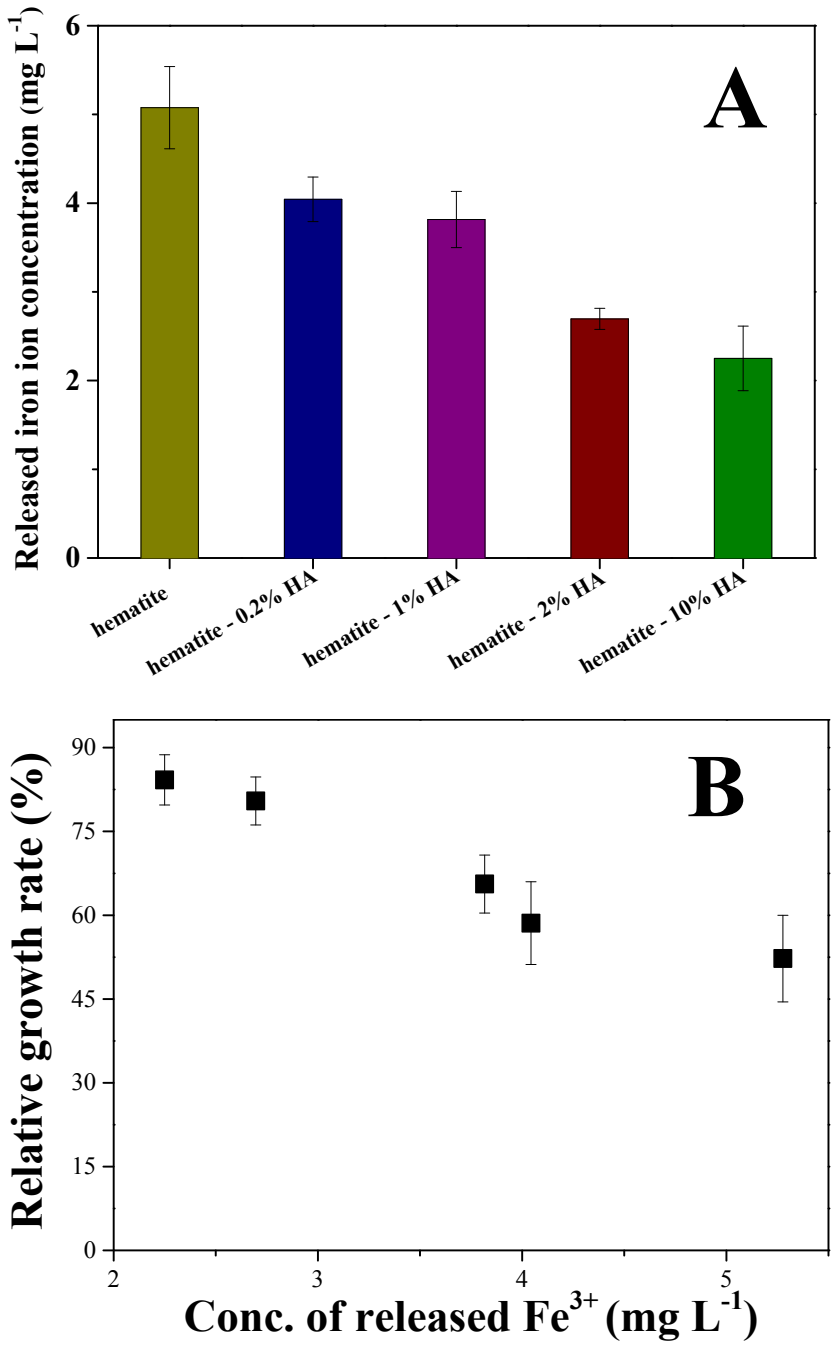

Figure S7 (A) The dissolution of Fe^{3+} ions released from hematite and hematite-HA complex systems in MMD medium. (B) The effect of released Fe^{3+} ions on the growth of *P. putida KT2440.* Each data point is the average of three replicates, with error bars denoting the standard deviation. The abscissa in (B) is the concentration of hematite-10%HA, hematite-2%HA, hematite-1%HA, hematite-0.2%HA, and hematite, respectively, from left to right.

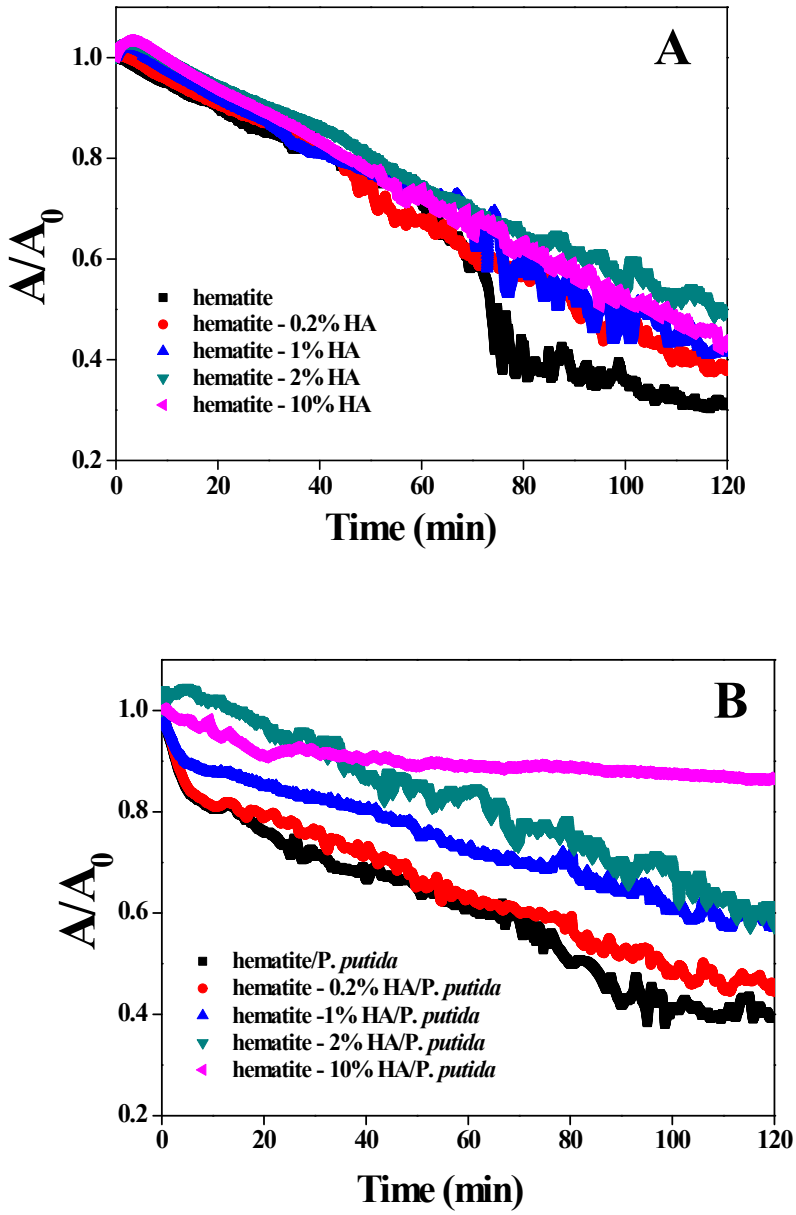

Figure S8 Settling curves of 50 mg L^{-1} of hematite and the hematite-HA complexes in the MMD medium in the absence (A) or presence (B) of the *P. putida* cells. A/A_0 is the ratio of absorbance at 660 nm of the test suspension at a given settling time to its initial absorbance.

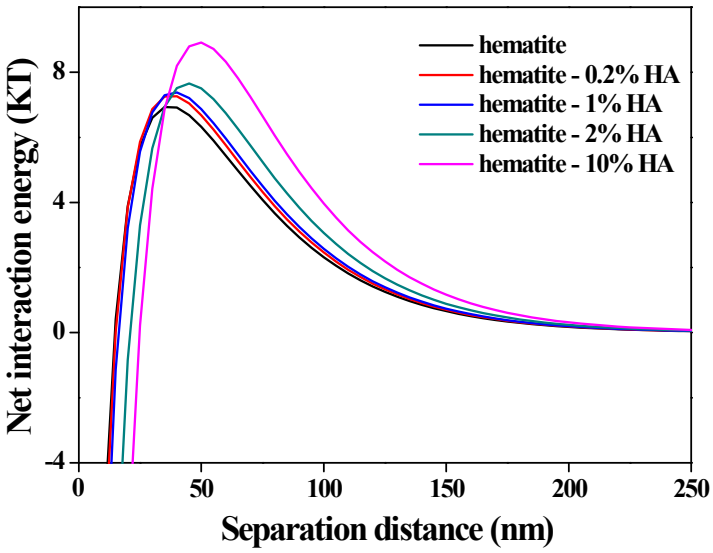

Figure S9 Net interaction energy profiles between *P. putida* and hematite, hematite-HA complexes.

REFERENCES

(1) Lin, D. H.; Tian, X. L.; Li, T. T.; Zhang, Z. Y.; He, X.; Xing, B. S. Surface bound humic acid increased Pb^{2+} sorption on carbon nanotubes. *Environ. Pollut.* **2012**, *167*, 138–47.

(2) Kaweeteerawat, C.; Ivask, A.; Liu, R.; Zhang, H. Y.; Chang, C. H.; Low-Kam, C.; Fischer, H.; Ji, Z. X.; Pokhrel, S.; Cohen, Y.; Telesca, D.; Zink, J.; Madler, L.; Holden, P. A.; Nel, A.; Godwin, H. Toxicity of metal oxide nanoparticles in *Escherichia coli* correlates with conduction band and hydration energies. *Environ. Sci. Technol.* **2015**, *49*, 1105−1112.

(3) Saison, C.; Perreault, F.; Daigle, J.; Fortin, C.; Claverie, J.; Morin, M.; Popovic, R. Effect of core-shell copper oxide nanoparticles on cell culture morphology and photosynthesis (photosystem II energy distribution) in the green alga, *Chlamydomonas reinhardtii*. *Aquat. Toxicol.* **2010**, *96*, 109–114.

(4) Hong, Y.; Hu, H.; Xie, X.; Sakoda, A.; Sagehashi, M.; Li, F. Gramine-induced growth inhibition, oxidative damage and antioxidant responses in freshwater cyanobacterium *Microcystis aeruginosa*. *Aquat. Toxicol.* **2009**, *91*, 262–269.

(5) Gurr, J. R.; Wang, A. S. S.; Chen, C. H.; Jan, K. Y. Ultrafine titanium dioxide particles in the absence of photoactivation can induce oxidative damage to human bronchial epithelial cells. *Toxicology* **2005**, *213*, 66-73

(6) Kumari, S. S.; Varghese, A.; Muraleedharan, D.; Menon, V. P. Effect of vitamin E on the severity of myocardial infarction induced by isoproterenol. *Indian J. Med. Res.* **1989**, *90*, 468–471.

(7) Stuart, B. H. Infrared Spectroscopy: Fundamentals and Applications. (Wiley,

England, **2004**), p. 143.

(8) Battisha, J. K.; Afify, H. H.; Ibrahim M. Synthesis of Fe_2O_3 concentrations and sintering temperature on FTIR and magnetic susceptibility measured from 4 to 300 K of monolith silica gel prepared by sol–gel technique. *J. Magn. Magn. Mater.* **2006**, *306*, 211-217.